Vortex Simulation of a Turbulent Mixing Layer

Osamu Inoue*
Institute of Space and Astronautical Science, Tokyo, Japan

Two-dimensional, turbulent mixing layers are numerically simulated by a vortex blob method. Streaklines of marker particles as well as those of vortices are obtained. The results indicate that not only a vortex pairing process, but also the self-growth of large eddies found by Hernan and Jimenez, play important roles in the development of a mixing layer. Streaklines of marker particles clearly show the entrainment process: nonturbulent fluid particles are entrained into the mixing layer between clusters of vortices because the nonturbulent outer flow acquires a normal velocity that is induced by clusters of vortices via the Biot-Savart law. Fluid particles in the slower-speed flow enter the mixing layer at a shorter downstream distance. Statistical quantities up to the second-order moment show similarity and reasonable agreement with experiments.

Introduction

THE existence of large scale, quasiordered, coherent structures in many types of turbulent flows, especially in the mixing layer, has been well recognized. Observation of the turbulent mixing layer by Brown and Roshko[1] and Winant and Browand[2] clearly showed that the mixing layer consists of a row of quasi two-dimensional coherent structures. Their work suggests that the amalgamation of the structures into larger ones ("vortex pairing") may produce the growth of the mixing layer. These observations suggest that representing turbulence as a superposition of interacting vortices may be a valid and useful idea. Many theoretical and numerical studies based on this idea have been made. They are reviewed by Saffman and Baker,[3] Leonard,[4] and Aref.[5] Readers are also referred to Roshko[6] and Cantwell[7] for reviews of the mixing layer.

Numerical simulation of a turbulent mixing layer by a discrete vortex method is based on this idea. In these studies, the mixing layers are represented as an assembly of two-dimensional, inviscid discrete vortices. It is generally accepted that the Reynolds number effect on the formation and development of large-scale coherent structure is secondary. The assumption of the two-dimensionality of the large-scale structure is supported by many experiments,[1,8] although it is not universally accepted when the freestream turbulence level is high or when the boundary layer on the splitter plate is turbulent.[9,10] Thus, the simulation of the mixing layer by discrete vortex method is quite reasonable and acceptable.

Simulation of the mixing layer by a discrete vortex method can be divided into two different approaches. In the first, the mixing layer is replaced by the time-developing shear layer whose coordinate system is moving with the convection velocity U_c. At an initial instant, vortices distributed in a finite region under periodic boundary conditions are disturbed. Our interest here lies in the time evolution of the distribution of the vortices. Results by this method often give good qualitative agreement with experiment.[11,12] The simulation of the mixing layer in this way, however, has several crucial disadvantages. The effects of both the convection velocity U_c and of the parameter $\lambda=(U_1-U_2)/(U_1+U_2)$, which has been considered important in the analysis of the mixing layer,[1,12] cannot be incorporated in the computation because the coordinate system is moving with the convection velocity U_c and the only characteristic velocity is the velocity difference ΔU $(=U_1-U_2)$. This makes it difficult to quantitatively compare the calculated and experimental results.

In the second approach, the spatially growing mixing layer is simulated directly. Vortices are shed one by one at every time step at a given point, such as the end of a virtual splitter plate. The strength of each vortex is determined from the velocity difference ΔU. The velocity of each vortex is calculated at every time step by directly summing the velocity field induced by individual discrete vortices, in addition to the contribution of the convection velocity U_c. With N vortices, this algorithm (direct summation method) requires evaluation of the order N^2 terms per time step and therefore is very time consuming for large N. Understandably, very few studies with large N have been made until now, except for the pioneering work of Ashurst.[13] Use of the cloud-in-cell method results in less computing time compared with the direct summation method. However, flow features of smaller scale than the grid cannot be accurately resolved if the cloud-in-cell method is used.

In spite of the disadvantage of the direct summation method, the simulation of a turbulent mixing layer in the second approach appears to be more faithful to the actual flow; most of the important parameters including λ are incorporated and excess conditions (grid, periodic boundaries, etc.) are excluded. In the present paper, simulation of the mixing layer with the second approach is adopted. The purpose of this paper is to numerically investigate a mixing layer with a high Reynolds number in order to increase our understanding of the turbulent mixing layer.

Mathematical Formulation and Numerical Procedure

Let us consider the flow produced by an infinite row of discrete vortices of the same sign and strength moving along the x axis with a constant velocity. If the circulation of a vortex is denoted by Γ, the distance between the two neighboring vortices by ℓ (= const), the constant velocity by U_c, and the upper- and lower-side velocities of the flow far from the x axis by U_1 and U_2, respectively, then the following relations are given:

$$\Gamma=\Delta U\cdot\ell \tag{1}$$

$$\Delta U=U_1-U_2 \tag{2}$$

$$U_c=(U_1+U_2)/2 \tag{3}$$

Next, let us suppose that at an initial instance, say $t=0$, vortices on the right-hand side ($x>0$) are suddenly removed. At all subsequent times, the vortices on the left-hand side ($x<0$) are assumed to continue to move along the x axis with

Received Aug. 11, 1983; revision received Feb. 25, 1984.

*Research Associate. Member AIAA.

the convection velocity U_c, as shown in Fig. 1. After reaching the origin ($x=0$), all vortices are assumed to move under the influence of the potential field induced by the individual vortices, with the contribution of the convection velocity. Our main interest lies in the motion of the discrete vortices to the right of the origin. At the initial stage of time development, the vortices may roll up into concentrated forms, which are convected downstream at the velocities approximately equal to U_c. After a sufficient time evolution, the turbulent mixing layer to be simulated may begin to form near the origin, where the effects of the rolled up vortices do not reach. The region where the mixing layer is formed tends to grow toward downstream with time. The complex velocity potential f, which governs the flow development, is then given by

$$f=U_c\cdot z+\sum_{n=1}^{N} i(2\pi)^{-1}\cdot\Gamma\cdot\log(z-z_n) \tag{4}$$

where $z=x+iy$. The velocity component u in the x direction and v in the y direction are given by

$$u-iv=\frac{\partial f}{\partial z} \tag{5}$$

The time development of an individual vortex is determined from the relation,

$$\frac{dx_n}{dt}=u_n \tag{6}$$

$$\frac{dy_n}{dt}=v_n \tag{7}$$

In this simulation the first-order Euler scheme is employed as a time integral scheme; that is,

$$x_n(t+\delta t)=x_n(t)+u_n(t)\cdot\delta t+\mathcal{O}(\delta t^2) \tag{8}$$

The advantage of this scheme is as follows. First, the computing time required for the evaluation of Eqs. (6) and (7) is much less than other schemes of higher-order accuracy. Second, the scheme inevitably introduces a viscous effect to the motion of the vortices. Recent investigations of discrete vortex methods has revealed that the numerical errors caused by the time integration introduces a viscous effect to the motion of discrete vortices. Theoretically, the time derivative of the second moment of the vorticity is proportional to the viscosity,

$$\frac{d}{dt}\iint\omega r^2\,dxdy=4\nu\iint\omega\,dxdy \tag{9}$$

where $r^2=x^2+y^2$ and ω is the vorticity. If the fluid is inviscid, the left-hand term should be exactly equal to zero. In actuality, however, this term does not vanish because of the effect of the time integration error. This error may be estimated by calculating the effective viscosity derived from Eq. (9) as

$$\nu_{\text{eff}}=\frac{1}{4}\frac{d}{dt}\sum_{n=1}^{N}\Gamma_n r_n^2\Big/\sum_{n=1}^{N}\Gamma_n \tag{10}$$

The effective viscosity ν_{eff} was recently estimated by Nakamura et al.[14] According to them, the effective viscosity ν_{eff} is proportional to δt for the first-order Euler method and to $(\delta t)^5$ for the fourth-order Runge-Kutta method. Thus, the lower-order time integral schemes enhance the viscous effect for the motion of the vortices. A similar effect caused by the difference in time integral scheme had been pointed out by Delcourt and Brown.[15] However, it should be emphasized that, as pointed out by Kuwahara and Takami,[16] the viscosity caused by numerical errors is actually similar to the turbulent viscosity rather than to the molecular viscosity. Thus, by using the Euler scheme, we simulate high Reynolds number flows with turbulent diffusion.

In order to save computing time, the upstream semi-infinite row of discrete vortices is replaced by 400 vortices. Preliminary tests showed that the effect of the difference between the use of 400 vortices and 800 vortices on the flow feature was insignificant.

The parameters used are:

$$U_c=3.2,\qquad \delta t=0.1 \text{ and } 0.2,\qquad \ell=U_c\cdot\delta t$$

$$\Gamma=0.512 \text{ for } \delta t=0.1 \text{ and } 1.024 \text{ for } \delta t=0.2$$

Thus, from Eqs. (1-3),

$$\Delta U=U_1-U_2=1.6,\qquad r=U_2/U_1=0.6$$

$$\lambda=(U_1-U_2)/(U_1+U_2)=0.25$$

The above parameters are prescribed by taking into consideration the experiments of Inoue et al.[17] and Oster and Wygnanski.[18] It should be noted that calculated values of the upper- and lower-side velocities far from the x axis are not exactly equal to the above U_1 and U_2, but they are close to each other. In order to avoid the singular behavior that occurs when two discrete vortices come very close, a core function of the following form was used:

$$u\propto\sum_{n=1}^{N}\frac{y-y_n}{(x-x_n)^2+(y-y_n)^2+\epsilon^2}$$

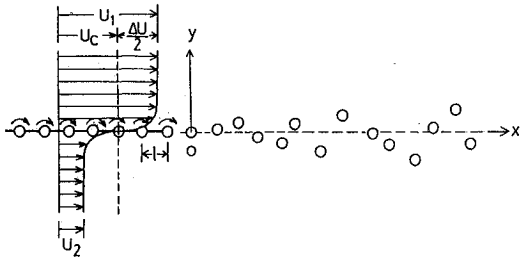

Fig. 1 Schematic of flow model.

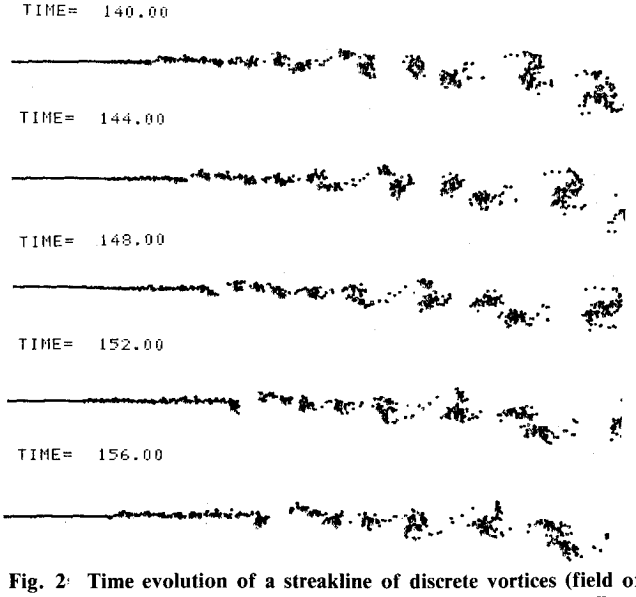

Fig. 2 Time evolution of a streakline of discrete vortices (field of view $0\le x\le 250$, upper flow has a higher speed than lower flow, $\epsilon=0.6\ell$, $\delta t=0.1$).

The constant ϵ was prescribed to be $\epsilon = 0.6$, 0.3, or 0.15ℓ. The effects of the core radius ϵ as well as the time step δt on the flow features will be discussed later. The computing time was less than 7 h case on the FACOM M-200 (the speed of M-200 is about the same as CDC-7600) with approximately 2600 vortices and 3000 marker particles.

Results and Discussion

Flow Visualization

So far as visual observation is concerned, the characteristic flow features described below were unchanged regardless of the core radius ϵ and the time step δt. Thus, we will discuss here only the results for the case of $\epsilon = 0.6\ell$ and $\delta t = 0.1$.

As mentioned in the previous section, at the initial stage of time development, vortices leaving the origin roll up into concentrated swirls. These are convected downstream with a velocity approximately equal to U_c. After a sufficient time evolution, the mixing layer is independent from the effect of the initial roll up. In the present calculation, the quasisteady mixing layer was formed in a region of $0 \le x \le 250$ after approximately $t = 100$. Here, the term "quasisteady" means that the profile of the mean velocity U shows similarity. Hereafter, our main interests lie in the region where the quasisteady mixing layer is formed.

A time evolution of a streakline of discrete vortices in the case of $\epsilon = 0.6\ell$ and $\delta t = 0.1$ is presented in Fig. 2, in which the field of view covers the region $0 < x < 250$. In this figure the upper flow has the higher velocity, while the lower flow has the slower velocity. It can readily be seen that there are two stages of vortex interaction. Immediately downstream of the origin (region I), discrete vortices interact with each other to form separate clusters of vortices (clustering process). Further downstream (region II), the clusters of discrete vortices thus formed interact with the other clusters and then rotate around each other to amalgamate into larger clusters of vortices (the vortex pairing process). After amalgamation, the clusters of discrete vortices interact with other clusters and amalgamate into further larger clusters. This vortex pairing process can be seen everywhere in region II.

In order to facilitate the comparison of flow visualization with experiments and also to observe the entrainment process, marker particles were introduced into the flowfield from three positions, at $y = 0$ and ± 5 on the y axis ($x = 0$). The positions of $y = 5$ and -5 at $x = 0$ are, respectively, in the nonturbulent flow region outside of the mixing layer. Because the marker particles were introduced at every time step from the three positions, an instantaneous plot of positions of the marker particles gives three streaklines of fluid particles. The time evolution of the streaklines of the marker particles corresponding to those of the discrete vortices shown in Fig. 2 is presented in Fig. 3. In region I, where discrete vortices interact with each other to form clusters of vortices, the streaklines are not much disturbed; in region II, where the vortex pairing process is predominant, the streaklines are much disturbed and the so-called large-scale structures, reported in many experimental studies, can clearly be seen. The flow features are consistent with the experimental observations. In fact, the agreement of the flow visualization results with the experiments is striking. For example, shadowgraphs of the mixing layer downstream of the splitter plate taken by Bernal et al.[19] and a picture of the mixing layer produced by a screen taken with the smoke-wire method by Inoue et al.[17] are presented in Figs. 4 and 5, respectively. The vortex pairing process shown in Fig. 4 has been almost faithfully reproduced in region II of Fig. 3. The existence of region I is qualitatively confirmed by the picture shown in Fig. 5, where undisturbed and rather straight streaklines can be

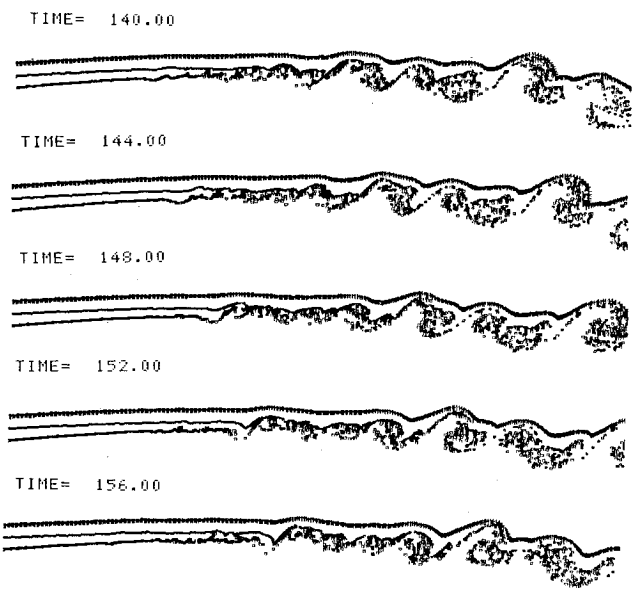

Fig. 3 Time evolution of the three streaklines of marker particles corresponding to Fig. 2 (each line starts at $y = 5$, 0, -5, respectively, on y axis ($x = 0$), $\epsilon = 0.6\ell$, $\delta t = 0.1$).

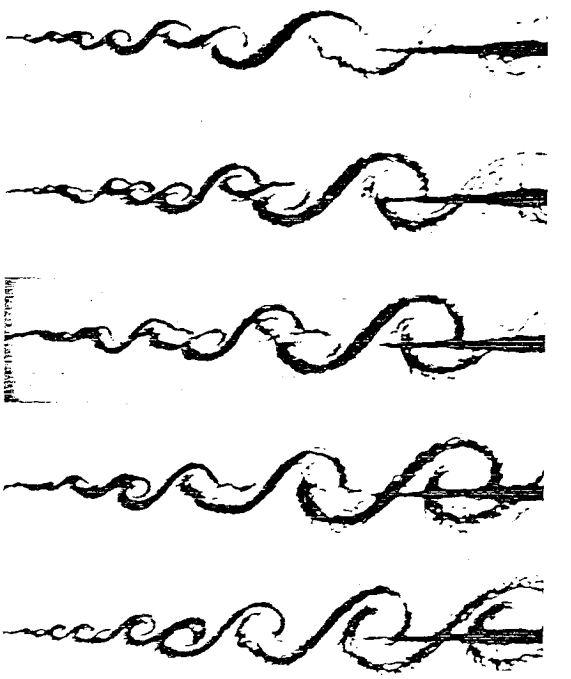

Fig. 4 Sequence of shadowgraphs showing pairing of vortices in a mixing layer, $U_1 = 10$ m/s and $U_2 = 3.5$ m/s (from Ref. 19).

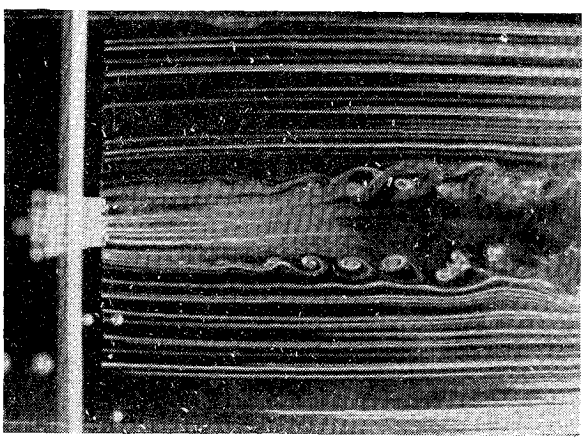

Fig. 5 Streaklines of paraffin smoke introduced into a mixing layer produced by a screen, $U_1 = 3.3$ m/s and $U_2 = 1.4$ m/s (from Ref. 17).

seen upstream of the large-scale structures. The nonexistence of region I in Fig. 4 may be due to the effect of the boundary layer that developed on the splitter plate; that is, the clustering process may have already occurred in the boundary layer.

The entrainment process of nonturbulent fluid particles into the turbulent flow region can also be observed from the streaklines of fluid particles shown in Fig. 3. In region I entrainment may not occur or proceeds very gradually if it does. In region II the entrainment process proceeds rapidly, owing to the existence of the clusters of vortices. In order to understand the entrainment process, it is better to observe the streaklines of both the discrete vortices and marker particles simultaneously. The streaklines of the discrete vortices and marker particles at time $t=156.0$ are shown in Fig. 6, in which the field of view is moved slightly downstream, say to $60\leq x\leq 310$. In the lower part of the figure, the three streaklines of the marker particles are also shown separately, where, for example, the symbol "$y=5.0$" denotes the streakline introduced into the mixing layer from the position of $y=5.0$ on the y axis. It can be seen here that the positions of the large-scale structures agree with the positions of the clusters of discrete vortices. The nonturbulent flows are entrained between the clusters of vortices into the mixing layer. The marker particles in the freestream with the higher velocity are entrained from the downstream side of a cluster of discrete vortices, while the marker particles with lower velocities are entrained from the upstream side. This result indicates that the nonturbulent fluid particles are entrained into the mixing layer because they acquire a normal velocity component that is induced by clusters of vortices via the Biot-Savart law. The three separate streaklines show that the marker particles with the lower velocity are entrained at a shorter downstream distance than the marker particles with the higher velocity.

Ashurst[13] simulated mixing layers with low and high Reynolds numbers by the direct summation method. He used a random walk in order to introduce the molecular-viscous effect and presented streaklines of discrete vortices for two different Reynolds numbers, $Re=250$ and 1000. He concluded that "the vortex pairing process is the mixing layer growth and is very important to the entrainment process of the surrounding nonturbulent fluid."

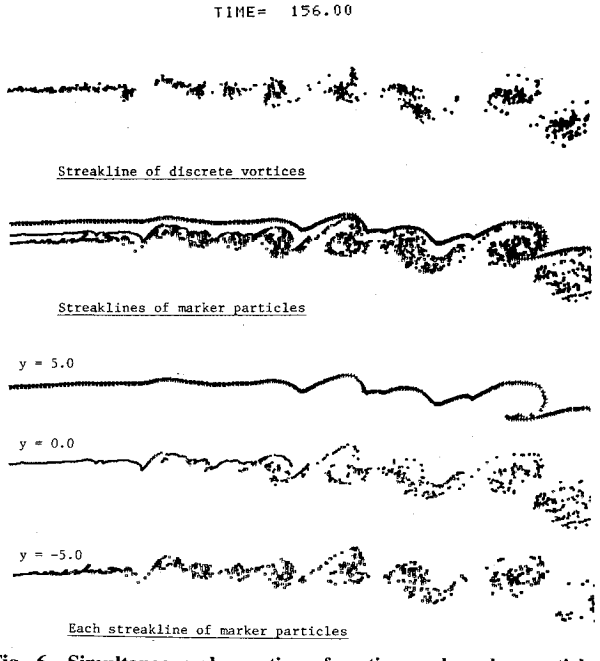

Fig. 6 Simultaneous observation of vortices and marker particles at an instance $t=156.0$ and separate presentation of the three streaklines of marker particles.

Flow features calculated by Ashurst are quite similar to those by the present calculation. Our conclusion is, however, slightly different from Ashurst's. As mentioned before, the entrainment occurs simply because the clusters of discrete vortices induce a nonzero normal velocity on nonturbulent flows, regardless of the vortex pairing process. The vortex pairing process serves to increase the strength of the vorticity of clusters of vortices by amalgamation. During the pairing process, centers of pairing clusters deviate from each other in the y direction and the effect of the potential field induced by the clusters reaches farther in the y direction. Therefore, it is true that more fluid particles are entrained during the pairing process, but this is merely a part of the entrainment process. Hernan and Jimenez[20] digitally analyzed Brown and Roshko's motion pictures and attributed most of the growth of the mixing layer to the growth of the large eddies in themselves rather than to the vortex pairing process. The present results also suggest the importance of this self-growth of large eddies because the entrainment occurs regardless of the pairing process. Thus, a mixing layer seems to grow because the nonturbulent outer flow is entrained into the mixing layer via the Biot-Savart law. The role of the vortex pairing process is to increase the strength of vorticity of clusters of vortices.

Aref and Siggia[12] simulated a shear layer by using the cloud-in-cell method. Their results showed the vortex pairing process, as in Ashurst's calculation, but also showed that the centers of vorticity, produced by clusters of discrete vortices, scatter about the midline ($y=0$) more and more with the increase in the thickness of the shear layer. They suggested that the shear layer may be thickened by a scattering of the vortex structure and only partly by vortex amalgamation.

A scattering of clusters of vortices, which somewhat resembles the scattering of vortex structures about the midline mentioned by Aref and Siggia, can be seen in Fig. 2, but these are all relevant to the vortex pairing process. They used a time integral scheme of fourth-order accuracy and viscous effects were hardly introduced into their calculation. In their view, the scattering of the vortex structure about the midline becomes predominant as the Reynolds number increases but experimental supporting evidence is scarce. Here it should be remembered that the viscosity caused by numerical errors has a similar property to the turbulent viscosity rather than the molecular viscosity. Kuwahara and Takami[16] simulated an inviscid motion of two clusters of discrete vortices that were initially located at a relatively large distance from each other. Their results clearly showed that vortex amalgamation is apt to occur if the first-order accurate Euler scheme is used, while it is not if the fourth-order accurate Runge-Kutta scheme is used. They suggested that turbulent viscosity may play an important role in vortex pairing process and that fourth-order

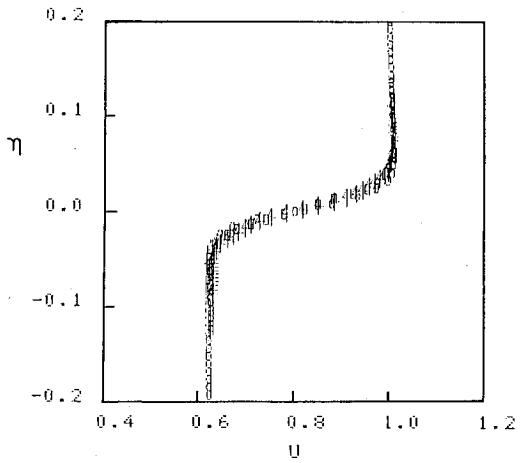

Fig. 7 Mean velocity profile at averaging time $120.0\leq t\leq 220.0$, $\epsilon=0.6\ell$, and $\delta t=0.1$ (○ $x=120$, □ $x=160$, + $x=200$).

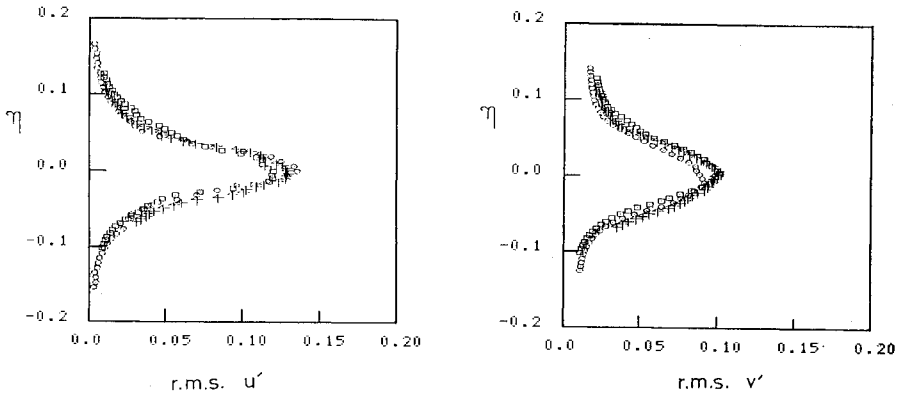

Fig. 8 Profiles of longitudinal and normal fluctuation velocities (for legend, see Fig. 7).

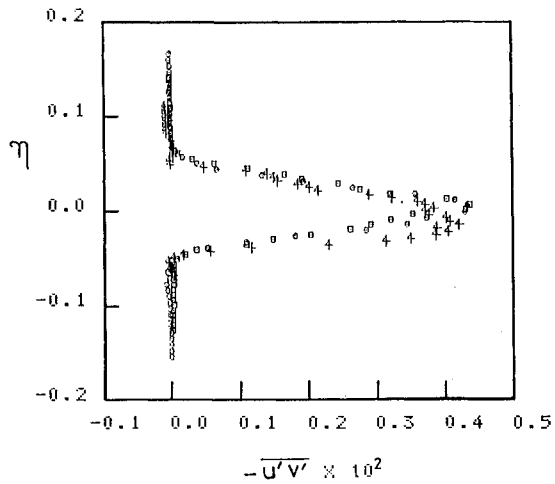

Fig. 9 Reynolds stress profile (for legend, see Fig. 7).

accurate time-integral schemes may be less adequate to simulate actual flows with turbulent diffusion when compared with the first-order Euler scheme. The disagreement between Aref and Siggia's results with many of the experimental observations may possibly be due to their time-integral scheme rather than to the Reynolds number effect.

Velocity Profile

Time-averaged profiles of the mean velocity, fluctuation velocities, and Reynolds stress in the case of $\epsilon=0.6\ell$ and $\delta t=0.1$ are presented in Figs. 7-9, respectively. They are obtained by averaging the instantaneous velocity profiles over the time $120.0\le t\le 220.0$ after a quasisteady mixing layer is formed in the region $0\le x\le 250$. In the figures, the velocities are made dimensionless by dividing by the freestream velocity U_1 and η is a similarity parameter defined by $\eta=(y-y_0)/(x-x_0)$.[1,21] The symbol $y_0(x)$ denotes a position where the mean velocity U is equal to $(U_1+U_2)/2$. The symbol x_0 denotes a virtual origin, which is assumed here to be zero.

The mean velocity profile shown in Fig. 7 shows the similarity and therefore indicates that the flow is in a self-preserving state. For the similarity of the mean velocity, however, a relatively short time was necessary for averaging, while the other higher-order quantities need a much longer averaging time. Therefore, the similarity of the mean velocity profile is not considered to be a sensitive test of self-preservation, an observation which has already been made by Aref and Siggia.

The profiles of fluctuating velocity, say rms u' and rms v', are shown in Fig. 8. In the calculation of Aref and Siggia, the normal velocity fluctuation (rms v') was larger than the longitudinal fluctuation (rms u'), which is contradictory to experimental results when the Reynolds number is high. They attributed this disagreement to the effect of the non-negligible three-dimensionality that exists in actual flows. This is apparently misleading, as easily seen from Fig. 8 in which the longitudinal velocity fluctuations are larger than the normal fluctuations. In Ashurst's calculation of low Reynolds number flow, both longitudinal and normal fluctuations showed the same magnitude, although an experiment has shown that in low Reynolds number flow the normal velocity fluctuations are larger than the longitudinal ones.[22] In order to overcome the problem, Ashurst had to introduce further viscous effect to the calculation, in addition to the random walk. In the present calculation, no difficulties arose in obtaining the fluctuation velocities. (See also Table 1 and Fig. 12 below.)

The profiles of the mean and the fluctuation velocities show the similarity very well. Although the data show some scatter, the profile of the Reynolds stress also shows reasonable similarity. The scatter in the data of the Reynolds stress is, we believe, due to insufficient averaging time, because the present calculation showed a tendency that the higher-order moments need longer averaging times. We actually calculated moments up to the third order, whose profiles are presented in Figs. 10 and 11. Although the qualitative features of the moments agree quite well with experiments,[21] the profiles are far from similar for time averaging, for say $120\le t\le 220$. (The profile of $\overline{u'^3}$ seems to be similar at first glance, but the values are seven to eight times larger than experimental values.) Better results could be obtained by doing a longer-time average, but this is costly in computer time.

A comparison of our calculated data of statistical quantities with experiments is presented in Table 1. The most important parameter in analyzing the mixing layer may be the velocity ratio $r=U_2/U_1$ or equivalently $\lambda=(U_1-U_2)/(U_1+U_2)$, although recent experiments indicate that the freestream turbulence level and initial states of the mixing layer may also be important.[9,10,17,18] Statistical quantities, especially the rate of growth of a mixing layer, depend on r or λ. Although many experiments concerning the plane mixing layer have been made, experiments in which the velocity ratio r is equal to 0.6 were selected for the present evaluation. In Table 1, δ_w denotes the vorticity thickness growth rate defined by $\delta_w=(U_1-U_2)/(\partial u/\partial y)_{\max}$ and $q^2=(u'^2_{\max}+v'^2_{\max}+w'^2_{\max})/U_1^2/2$. From the table, one can readily see the following. First, in each of the five cases presented, the calculated data show larger values than those of the experiment; the maximum difference between them is about 50% of the larger value. Second, the effect of core radius on the flow features is slight (cases 1-3). This is more clearly seen in Fig. 12, where the dependence of the growth rate of a mixing layer and also that of the rms velocities on the core radius are presented with their error bars. The quantities fall within their respective error ranges. One can also see from Fig. 12 that rms u' is larger than rms v' regardless of the core radius. Third, the larger time step seems to increase rms u' values, while decreasing rms v' values

Table 1 Comparison of statistical quantities with experiments $[r=0.6, \lambda=0.25, q^2=(u'^2_{\max}+v'^2_{\max}+w'^2_{\max})/U_1^2/2]$

	δt	ϵ	$\frac{\delta_w}{x-x_0}$	$\left(\frac{u'}{U_1}\right)_{\max}$	$\left(\frac{v'}{U_1}\right)_{\max}$	$\left(\frac{w'}{U_1}\right)_{\max}$	$-\left(\frac{u'v'}{U_1^2}\right)_{\max}$	q^2
Oster and Wygnanski[18]			0.045	0.072	0.061	0.058	0.21×10^{-2}	0.62×10^{-2}
Yule[23]			0.054	0.069	0.064	0.072	0.21×10^{-2}	0.70×10^{-2}
Spencer[24]			?	0.068	0.056	0.058	0.18×10^{-2}	0.56×10^{-2}
Calculated								
Case 1	0.1	0.6ℓ	0.060	0.126	0.100	—	0.41×10^{-2}	1.29×10^{-2}
Case 2	0.1	0.3ℓ	0.050	0.134	0.095	—	0.32×10^{-2}	1.35×10^{-2}
Case 3	0.1	0.15ℓ	0.055	0.130	0.093	—	0.38×10^{-2}	1.27×10^{-2}
Case 4	0.2	0.6ℓ	0.047	0.142	0.083	—	Not similar	1.37×10^{-2}
Case 5	0.2	0.3ℓ	0.049	0.139	0.079	—	Not similar	1.28×10^{-2}

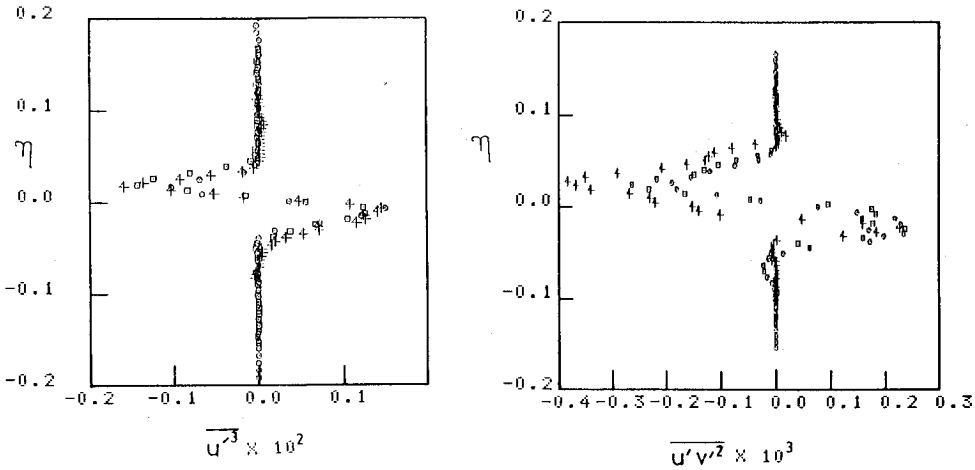

Fig. 10 Profiles of third-order moments (1) (for legend, see Fig. 7).

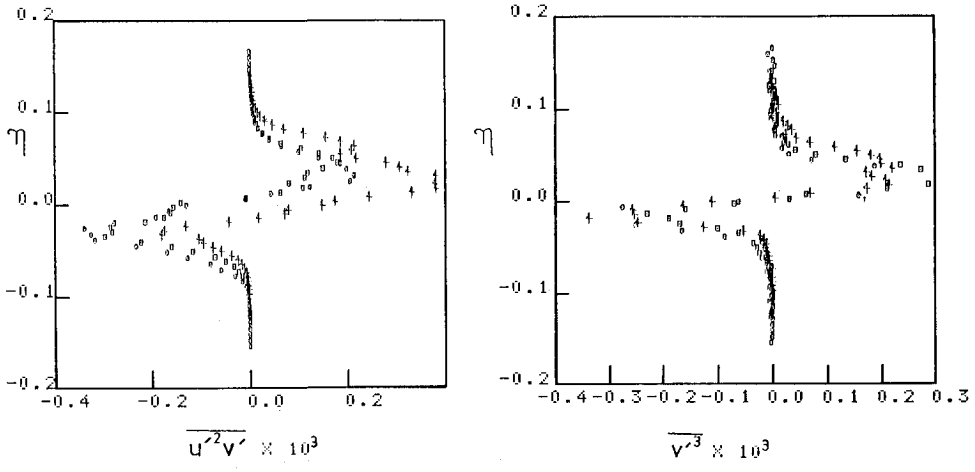

Fig. 11 Profiles of third-order moments (2) (for legend, see Fig. 7).

(cases 4 and 5). The rms u' value with further larger time-step ($\delta t=0.4$) also leads to a similar result, although the result is not shown here. It should be noted, however, that for the averaging time, say $120\le t\le220$, the profiels of the Reynolds stress for the cases of $\delta t=0.2$ (cases 4 and 5) measured at several x stations did not show similarity. For the cases of $\delta t=0.4$, rms v' as well as the Reynolds stress did not show similarity. Therefore, the present results concerning the effect of the time step on the flow features should be considered inconclusive. Calculated data using smaller time steps are required, but this is costly.

From the above results, the following reasons for the overestimation by the calculation may be considered: 1) the effect of non-negligible three-dimensionality existing in actual flows, as seen from the values of $(w'/U_1)_{\max}$ in Table 1, which are comparable with or even larger than the values of $(v'/U_1)_{\max}$; and 2) the effect of the time step.

In order to check the effect of three-dimensionality, we calculated q^2 , which may give an estimate of turbulence energy. If the values of q^2 are the same as or nearly equal to each other, calculated values of $(u'/U_1)_{\max}$ and $(v'/U_1)_{\max}$ should be larger than the experimental ones, because the present calculation entirely neglects the three-dimensionality (i.e., $w'=0$). As seen from Table 1, however, the calculated values of q^2 are approximately twice as large as the experimental ones. Therefore, the overestimation of the statistical quantities in this calculation may not readily be attributed to the three-dimensionality effect. The effect of time-step may also remain as one of the main causes of the discrepancy between the calculated and experimental results. However, the maximum ratio between the calculated and experimental values is at most two and further improvement of the values, under the assumption of two-dimensionality, may not be very important because the three-dimensionality

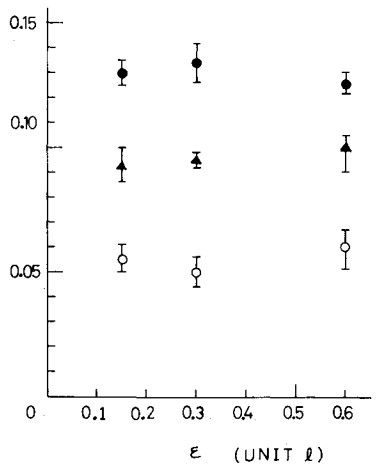

Fig. 12 Effect of core radius ϵ, $r=0.6$, $\delta t=0.1$ (○ $\delta_w/(x-x_0)$, ● $(u'/U_1)_{max}$, ▲ $(v'/U_1)_{max}$).

existing in actual flows cannot be taken into account and a perfect agreement between calculated and experimental values is basically impossible.

Summary and Conclusions

Two-dimensional, turbulent mixing layers with high Reynolds numbers were simulated by a vortex blob method. A turbulent mixing layer seems to be thickened simply because nonturbulent fluid particles are forced by clusters of discrete vortices or large eddies to have their normal velocity via the Biot-Savart law and are thus entrained into the mixing layer. The role of the vortex pairing process seems to increase the strength of vorticity of the clusters of discrete vortices. Thus, the self-growth of large eddies found by Hernan and Jimenez may also play an important role in development of a mixing layer. Statistical quantities calculated up to the second moment show similarity and give reasonably good agreement with experiments, at least for a small time step. The effect of the core radius on the flow features was slight. The effects of three-dimensionality and of the time step on the flow features remain an unsolved problem for a furture investigation.

Acknowledgments

The author expresses his sincere gratitude to Prof. H. Oguchi for many useful comments. He also owes much to Prof. K. Kuwahara for his useful advice and helpful discussions, especially on the use of the discrete vortex method. Thanks are also due to Dr. Wm. T. Ashurst for his valuable comments and suggestions on the first draft of this paper.

References

[1] Brown, G. L. and Roshko, A., "On Density Effects and Large Structures in Turbulent Mixing Layers," *Journal of Fluid Mechanics*, Vol. 64, 1974, pp. 775-816.

[2] Winant, D. and Browand, F. K., "Vortex Pairing: The Mechanism of Turbulent Mixing-Layer Growth at Moderate Reynolds Number," *Journal of Fluid Mechanics*, Vol. 63, 1974, pp. 237-255.

[3] Saffman, P. G. and Baker, G. R., "Vortex Interactions," *Annual Review of Fluid Mechanics*, Vol. 11, 1979, pp. 95-122.

[4] Leonard, A., "Vortex Methods for Flow Simulation," *Journal of Computational Physics*, Vol. 37, 1980, pp. 289-335.

[5] Aref, H., "Integrable Chaotic, and Turbulent Vortex Motion in Two-Dimensional Flows," *Annual Review of Fluid Mechanics*, Vol. 15, 1983, pp. 345-389.

[6] Roshko, A., "Structures of Turbulent Shear Flows: A New Look," *AIAA Journal*, Vol. 14, 1976, pp. 1349-1357.

[7] Cantwell, B. J., "Organized Motion in Turbulent Shear Flow," *Annual Review of Fluid Mechanics*, Vol. 13, 1981, pp. 457-515.

[8] Wygnanski, I., Oster, D., Fiedler, H. E., and Dziomba, B., "On the Perseverance of a Quasi-Two-Dimensional Eddy-Structure in a Turbulent Mixing Layer," *Journal of Fluid Mechanics*, Vol. 93, 1979, pp. 325-335.

[9] Chandrsuda, C., Mehta, R. D., Weir, A. D., and Bradshow, P., "Effect of Free-Stream Turbulence on Large Structure in Turbulent Mixing Layer," *Journal of Fluid Mechanics*, Vol. 85, 1978, pp. 693-704.

[10] Pui, N. K. and Gartshore, I. S., "Measurement of the Growth Rate and Structure in Plane Turbulent Mixing Layers," *Journal of Fluid Mechanics*, Vol. 91, 1979, pp. 111-130.

[11] Acton, E., "The Modeling of Large Eddies in a Two-Dimensional Shear Layer," *Journal of Fluid Mechanics*, Vol. 76, 1976, pp. 561-592.

[12] Aref, H. and Siggia, E. D., "Vortex Dynamics of the Two-Dimensional Turbulent Shear Layer," *Journal of Fluid Mechanics*, Vol. 100, 1980, pp. 705-737.

[13] Ashurst, W. T., "Numerical Simulation of Turbulent Mixing Layers via Vortex Dynamics," *Turbulent Shear Flows*, Vol. I, edited by Durst et al., Springer-Verlag, New York, 1979, pp. 402-413.

[14] Nakamura, Y., Leonard, A., and Spalart, P., "Vortex Simulation of an Inviscid Shear Layer," AIAA Paper 82-0948, 1982.

[15] Delcourt, B. A. G. and Brown, G. L., "The Evolution and Emerging Structure of a Vortex Sheet in an Inviscid and Viscous Fluid Modelled by a Point Vortex Method," *2nd Symposium on Turbulent Shear Flows*, Imperial College, London, 1979, p. 14.

[16] Kuwahara, K. and Takami, H.,, "Study of Turbulent Wake behind a Bluff Body by Vortex Method," *Proceedings of IUTAM Symposium on Turbulence and Chaotic Phenomena in Fluids*, edited by T. Tatsumi, North-Holland Publishing Corp., Amsterdam, 1983.

[17] Inoue, O., Sato, S., and Oguchi, H., "Flow Visualization and LDV Measurements of Turbulent Mixing Layer," Institute of Space and Astronautical Science, ISAS Rept. 606, 1983.

[18] Oster, D. and Wygnanski, I., "The Forced Mixing Layer Between Paralell Streams," *Journal of Fluid Mechanics*, Vol. 123, 1982, pp. 91-130.

[19] Bernal, L., Brown, G. L., and Roshko, A., *An Album of Fluid Motion*, edited by M. van Dyke, Parabolic Press, 1982, p. 103.

[20] Hernan, M. A. and Jimenez, J., "Computational Analysis of a High-Speed Film of the Plane Turbulent Mixing Layer," *Journal of Fluid Mechanics*, Vol. 119, 1982, pp. 323-345.

[21] Wygnanski, I. and Fiedler, H. E., "The Two-Dimensional Mixing Region," *Journal of Fluid Mechanics*, Vol. 41, 1970, pp. 327-361.

[22] Browand, F. K. and Weidman, P. D., "Large Scales in the Developing Mixing Layer," *Journal of Fluid Mechanics*, Vol. 76, 1976, pp. 127-145.

[23] Yule, A. J., Aeronautics Research Council, London, R&M 3683, 1971 (from Ref. 18).

[24] Spencer, B. W., Ph.D. Thesis, Nuclear Engineering Program, University of Illinois, Urbana, 1970 (from Ref. 18).